Interpreting 750 GeV Diphoton Excess with R-parity Violating Supersymmetry

Ran Ding,[1] Li Huang,[2] Tianjun Li,[2,3] and Bin Zhu[4]

[1] *Center for High-Energy Physics, Peking University, Beijing, 100871, P. R. China*
[2] *State Key Laboratory of Theoretical Physics and Kavli Institute for Theoretical Physics, China (KITPC), Institute of Theoretical Physics, Chinese Academy of Sciences, Beijing 100190, P. R. China*
[3] *School of Physical Electronics, University of Electronic Science and Technology of China, Chengdu 610054, P. R. China*
[4] *Institute of Physics Chinese Academy of sciences, Beijing 100190, P. R. China*

We propose an supersymmetric explanation of the diphoton excess in the Minimal Supersymmetric Standard Model with the leptonic R-parity violation. Where the sneutrino serves as the 750 GeV resonance and produced through quark anti-quark annihilation. With introducing appropriate trilinear soft parameters, we show that the diphoton branching ratio is significantly enhanced compared with the conventional MSSM. The parameter space favored by diphoton excess strongly indicates the mass of smuon and stau fall into the range $375 - 410$ (375-480) GeV, which depending on the electroweakino masses. In addition, the R-parity-violating trilinear couplings involved with second generation quarks are both favored by compatibility of diphoton excess and low-energy constraints.

arXiv:1512.06560v2 [hep-ph] 20 May 2016

1. Introduction–Recently, both ATLAS and CMS reported an excess on diphoton channel around the invariant mass $M \simeq 750$ GeV in the run II data of LHC at $\sqrt{s} = 13$ TeV. For ATLAS observation, the local significance of the excess reaches 3.9 σ with a best-fit width of about 45 GeV ($\Gamma/M \simeq 0.06$) [1]. While for CMS observation, the local significance is 2.6 σ and the best-fit prefers a narrow width [2]. The corresponding signal cross sections can be estimated as:

$$\sigma^{13\text{TeV}}_{pp\to\gamma\gamma} \simeq \begin{cases} (10 \pm 3)\text{ fb} & \text{for ATLAS [1]}, \\ (6 \pm 3)\text{ fb} & \text{for CMS [2]}. \end{cases} \quad (1)$$

Although it may be eventually identified as a fluctuation, the possibility of a new resonance is likely to be strong hints for new physics beyond the standard model (BSM). Which has inspired many model building efforts in various phenomenological frameworks [3–37].

One of the most intriguing problems is then whether or not this excess can be interpreted in the framework of Supersymmetry (SUSY). In this direction, current works focus on the heavy Higgs candidates in the Minimal Supersymmetric Standard Model (MSSM) and the Next-to-Minimal Supersymmetric Standard Model (NMSSM) [7]. Unfortunately, it is found that the diphoton branching ratio reaches only $\mathcal{O}(10^{-6})$ even in the case of $\tan\beta \sim 1$ which is the lower limit required by the Renormalization Group Equation (RGE) of Yukawa couplings. As a result, one has to introduce extra vector-like fermions to alleviate the discrepancy of diphoton rate between the model prediction and experimental requirement. In this paper, we suggest a novel approach to explain such excess without the need of any ad-hoc addition of extra particles. We consider the framework of Leptonic R-parity-violating (LRPV) MSSM, where the 750 GeV resonances is identified with the sneutrino and produced via quark anti-quark annihilation. The diphoton excess is then originated from its loop-induced decay. With introducing appropriate LRPV soft breaking trilinear terms, the diphoton branching ratio receives significant enhancement compared with conventional MSSM due to the contribution of sleptons in the loop.

The organization of paper is as follows: In section 2, we introduce our model and illustrate the mechanism of diphoton enchantment. In section 3, we then explore the parameter space in our model with taking into account relevant LHC limits and low-energy constraints. The last section is devoted to conclusion.

2. LRPV MSSM– We start with the superpotential of LRPV model [38]:

$$W = Y_d^{ij} Q_i H_d D_j^c + Y_u^{ij} Q_i H_u U_j^c + Y_e^{ij} L_i H_d E_j^c + \mu H_u H_d + \frac{1}{2}\lambda_1^{ijk} L_i L_j E_k^c + \lambda_2^{ijk} L_i Q_j D_k^c \ . \quad (2)$$

In above equation, the $SU(2)_L$ and $SU(3)_C$ indices have been suppressed. $i,\ j,\ k = 1,\ 2,\ 3$ are the the family indices and a summation is implied. Q_i (L_i) are the $SU(2)_L$ doublet quark (lepton) superfields. D_j^c and U_j^c (E_j^c) are the $SU(2)_L$ singlet down- and up-quark (electron) superfields, respectively. λ_1 and λ_2 are trilinear couplings. The lepton number is automatically violated by $\lambda_1^{ijk} L_i L_j E_k^c$ and $\lambda_2^{ijk} L_i Q_j D_k^c$ operators and the first term is anti-symmetric in i, j indices. In our model, sneutrino serves as 750 GeV resonance. We therefore only list the relevant soft interactions for sneutrino sector:

$$-L_{\text{soft}} = T_{\lambda_1}^{ijk} \tilde{\nu}_{iL} \tilde{e}_{jL} \tilde{e}_{kR}^* + T_{\lambda_2}^{ijk} \tilde{\nu}_{iL} \tilde{d}_{jL}^{\beta} \tilde{d}_{kR}^{*\gamma} \delta_{\beta\gamma} + \tilde{\nu}_{iL}^* (m_{\tilde{l}}^2)^{ij} \tilde{\nu}_{jL} \ , \quad (3)$$

where the fields with tilde denote the scalar fermion superpartners. As is shown in Eq. 2 and 3, the production and decay properties of sneutrino are determined by λ_1^{ijk}, λ_2^{ijk}, $T_{\lambda_1}^{ijk}$ and $T_{\lambda_2}^{ijk}$. Here we only consider the first generation sneutrino $\tilde{\nu}_e$ as a illustration. It is straightforward to include the other generations by multiplying a factor to the signal strength if one takes the degenerate mass spectrum. In order to compute the loop-induced decay $\tilde{\nu}_e \to \gamma\gamma$, we divide the sneutrino into its CP-even and CP-odd part,

$$\tilde{\nu}_e = \frac{1}{\sqrt{2}}(\tilde{\nu}_e^+ + i\tilde{\nu}_e^-). \quad (4)$$

We first investigate the contributions from fermionic loop. This calculation is analogous to the CP-even/odd neutral Higgs decay into diphoton and into di-gluon in the MSSM. One obtains following partial widths [39],

$$\Gamma(\tilde{\nu}_e^{\pm} \to \gamma\gamma) = \frac{\alpha^2 m^3_{\tilde{\nu}_e^{\pm}}}{512\pi^3} \left| \sum_{j=1}^{3} \frac{N_c}{m_{d_j}} e^2_{d_j} \lambda_2^{1jj} A^{\pm}_{1/2}(\tau_{d_j}) + \sum_{j=2}^{3} \frac{1}{m_{l_j}} \lambda_1^{1jj} A^{\pm}_{1/2}(\tau_{l_j}) \right|^2, \quad (5)$$

$$\Gamma(\tilde{\nu}_e^{\pm} \to gg) = \frac{\alpha_s^2 m^3_{\tilde{\nu}_e^{\pm}}}{256\pi^3} \left| \sum_{j=1}^{3} \frac{1}{m_{d_j}} \lambda_2^{1jj} A^{\pm}_{1/2}(\tau_{d_j}) \right|^2, \quad (6)$$

where the sum in Eq. 5 (Eq. 6) runs over all down-fermions (down–quarks). Furthermore, $N_c = 3$ is the number of colors and α (α_s) is the QED (QCD) fine structure constant. $e_{d_j} = -1/3$ is the electric charge of down-type quarks, $\tau = 4m^2/m^2_{\tilde{\nu}}$ with m the mass of particles running in loop. The loop function $A^{\pm}_{1/2}$ is given by [40],

$$\begin{aligned} A^{+}_{1/2} &= -2\tau(1 + (1-\tau)f(\tau)), \\ A^{-}_{1/2} &= -2\tau f(\tau), \\ f(\tau) &= \begin{cases} \arcsin^2[1/\sqrt{\tau}], & \text{if } \tau \geq 1 \\ -\frac{1}{4}[\ln \frac{1+\sqrt{1-\tau}}{1-\sqrt{1-\tau}} - i\pi]^2, & \text{if } \tau < 1. \end{cases} \end{aligned} \quad (7)$$

The structure of $A^{\pm}_{1/2}$ implies that $A^{\pm}_{1/2}/m \to 0$ when $m \to 0$. This feature indicates that loop contribution from quarks and leptons are highly suppressed except for the third generation, i.e., bottom quark and tau lepton. While including the contribution of third generation fermions also introduce a new decay modes like $\Gamma(\tilde{\nu} \to b\bar{b})$ and $\Gamma(\tilde{\nu} \to \tau^+\tau^-)$, which considerably suppress the branching ratio of diphoton mode. Moreover, the production of sneutrino through $b\bar{b}$ channel is expected to be much smaller than that of first two generation quarks. Due to the above reasons, we do not consider the case of third generation and assuming $j, k = 1, 2$ for λ_1^{1jk} and λ_2^{1jk}.

We then take into account contribution from sfermions. As we will show later, which plays a crucial role in diphoton enhancement. The decay modes in Eq. 5 and 6 can be safely neglected in this case. Notice that we can simply treated CP-even $\tilde{\nu}^+$ as the resonance since the sfermion loops can not give any contribution to CP-odd $\tilde{\nu}^-$. The corresponding partial widths are given by,

$$\delta\Gamma(\tilde{\nu}_e^{+} \to \gamma\gamma) = \frac{\alpha^2 m^3_{\tilde{\nu}_e^{\pm}}}{512\pi^3} \left| \sum_{j=1}^{3} \frac{N_c}{2m^2_{\tilde{d}_j}} e^2_{d_j} \sin 2\theta_2 T^{1jj}_{\lambda_2} A^{+}_{0}(\tau_{\tilde{d}_j}) + \sum_{j=2}^{3} \frac{1}{2m^2_{\tilde{l}_j}} T^{1jj}_{\lambda_1} \sin 2\theta_1 A^{+}_{0}(\tau_{\tilde{l}_j}) \right|^2, \quad (8)$$

$$\delta\Gamma(\tilde{\nu}_e^{+} \to gg) = \frac{\alpha_s^2 m^3_{\tilde{\nu}_e^{\pm}}}{256\pi^3} \left| \sum_{j=1}^{3} \frac{1}{2m^2_{\tilde{d}_j}} T^{1jj}_{\lambda_2} \sin 2\theta_2 A^{+}_{0}(\tau_{\tilde{d}_j}) \right|^2 \quad (9)$$

where

$$A^{+}_{0} = \tau(1 - \tau f(\tau)). \quad (10)$$

In this case, the mass eigenstates of sleptons (only second and third generations are involved since $T^{1jj}_{\lambda_2}$ is anti-symmetric in $1, j$ indices.) and squarks (can be both three generations) do not coincide with the gauge eigenstates due to introduce non-zero mixing trilinear terms. Here θ_1/θ_2 being the mixing angle between left-handed and right-handed slepton/squarks, respectively. In order to enhance diphoton partial width as much as possible, we assume maximal mixing scenario in this paper, i.e., setting $\theta_1 = \theta_2 = \pi/4$. As a consequence, the mass eigenstates tend to have a large splitting thus the contributions from heavier ones can be ignored in the loop calculation.

One immediately find that both $\delta\Gamma(\tilde{\nu}^+ \to \gamma\gamma)$ and $\delta\Gamma(\tilde{\nu}^+ \to gg)$ are proportional to $T_\lambda/m_{\tilde{f}}$. To enhance the diphoton partial width effectively, one thus prefers large soft trilinear term T_λ and relatively light sfermion. Unfortunately, the di-gluon partial width is also received enhancement in this way and the ratio of two modes is roughly estimated as α_s^2/α^2. As a result, the total effect of sfermion loops actually reduces the diphoton branching ratio. The simplest way to solve this dilemma is choose $T^{ijk}_{\lambda_2} = 0$, which forbidding the contribution of squarks and only leaving sleptons in the loop. One thus has

$$\Gamma_{\gamma\gamma} \equiv \delta\Gamma(\tilde{\nu}_e^{+} \to \gamma\gamma) = \frac{\alpha^2 m^3_{\tilde{\nu}_e^{\pm}}}{512\pi^3} \left| \sum_{j=2}^{3} \frac{1}{2m^2_{\tilde{l}_j}} T^{1jj}_{\lambda_1} \sin 2\theta_1 A^{+}_{0}(\tau_{\tilde{l}_j}) \right|^2, \quad (11)$$

and $\delta\Gamma(\tilde{\nu}_e^{+} \to gg) = 0$.

We finally obtain a valid recipe in LRPV MSSM which successfully enhances diphoton partial width while avoiding unwanted di-gluon mode.

In the rest of this section, we deal with other important decay modes of sneutrino:

- Decaying into first two generation di-quarks via LQD^c operator with the partial width,

$$\Gamma_{d\bar{d}} \equiv \Gamma(\tilde{\nu}_e^{+} \to d_j \bar{d}_k) = \frac{3}{16\pi} |\lambda_2^{1jk}|^2 m_{\tilde{\nu}_e^{+}}. \quad (12)$$

  It is the inverse process of sneutrino production thus unavoidable and dominates the branching ratios in general. This decay mode leads to dijet final states and impose stringent constraint on λ_2^{1jk}.

- Decaying into di-lepton via LLE^c operator, which is severely limited by LHC di-lepton resonance searches [47]. This decay mode can not be forbidden kinematically due to the lightness of leptons. We thus assuming λ_1^{ijk} is negligible to remove this dangerous mode.

- Decaying into squark and slepton pairs due to the soft trilinear terms $T_{\lambda_2}\tilde{\nu}_L\tilde{d}_L\tilde{d}_R^*$ and $T_{\lambda_1}\tilde{\nu}_L\tilde{e}_L\tilde{e}_R^*$, respectively. Among them, the di-squark mode is automatically vanished since we have taken $T_{\lambda_2}=0$. While for di-slepton mode, we must keep large T_{λ_1} since it is also responsible for enhancing the diphoton partial width. We therefore forbid di-slepton mode kinematically by setting $m_{\tilde{\mu},\tilde{\tau}} > 375$ GeV.

- Decaying into electroweakinos (neutrlinos and charginos) through gauge interaction. They have following partial widths [41]:

$$\begin{aligned}\Gamma_{\chi l} &\equiv \Gamma(\tilde{\nu}_e^+ \to \tilde{\chi}_a^0\nu_e, \tilde{\chi}_a^+ e^-) \\ &= \frac{Cg^2}{16\pi} m_{\tilde{\nu}_e^+}\left(1-\frac{m^2_{\tilde{\chi}_a^+}}{m^2_{\tilde{\nu}_e^+}}\right)^2 . \end{aligned} \tag{13}$$

  Where the coefficient $C=|N_{a2}|^2$ ($C=|V_{a1}|^2$) for the neutralinos (charginos) case. with N_{a2} and V_{a1} the elements of mixing matrix.

- Finally, decaying into neutral gauge bosons $Z\gamma$ and ZZ via the same loop diagram as the diphoton mode. However, their contributions to the total decay width are much smaller than other modes discussed above. We therefore neglect these two modes in the following discussion and numerical calculations.

In summary, one leaves three modes in the decay pattern of sneutrino: $\tilde{\nu}_e \to \gamma\gamma$ via slepton loops, $\tilde{\nu}_e \to d_j\bar{d}_k$ and $\tilde{\nu}_e \to \tilde{\chi}^0\nu_e, \tilde{\chi}^+e^-$. The total decay width is then $\Gamma_{\rm tot} = \Gamma_{\gamma\gamma}+\Gamma_{d\bar{d}}+\Gamma_{\chi l}$, with the branching ratio of diphoton and di-quark modes are respectively $\mathrm{BR}_{\gamma\gamma}=\Gamma_{\gamma\gamma}/\Gamma_{\rm tot}$ and $\mathrm{BR}_{d\bar{d}}=\Gamma_{d\bar{d}}/\Gamma_{\rm tot}$.

3. Diphoton excess and LHC constraints–In this section, we investigate the diphoton signal rate in our model. For this purpose, we use `SARAH` [42] to generate `UFO` model file [43], and `MadGraph5_aMC@NLO` [44] to calculate the production cross section of sneutrino with `CTEQ6L1` [45] parton distribution function (PDF). Based on the discussion in section 2, we have following input parameters: $[m_{\tilde{l}},\ m_{\tilde{\chi}^\pm}, m_{\tilde{\chi}^0},\ T_{\lambda_1}^{1jj},\ \lambda_2^{1jk}]$. Where the independent components of $T_{\lambda_1}^{1jj}$ and λ_2^{1jk} are $T_{\lambda_1}^{1jj}=T_{\lambda_1}^{122,133}$ and $\lambda_2^{1jk}=\lambda_2^{111,112,121,122}$, respectively.

Before showing our results, we make some comments on the choice of parameters in the numerical analysis. We work in the framework of simplified SUSY models, with only involving sleptons and electroweakinos in the mass spectrum. In this scenario, one can take either light or heavy electroweakinos, which has significant impact on the total decay width of sneutrino. The current LHC limits on RPV SUSY models are reviewed in Ref. [46]. Those related to our model are constraints on LLE^c and LQD^c interactions. For LLE^c operator, by assuming $\tilde{\chi}_1^0$ as a lightest supersymmetric particle (LSP) and using simplified models, one obtains following approximate upper bounds on superpartner masses:

- gluino masses $m_{\tilde{g}} > 950$ GeV,
- light stop masses $m_{\tilde{t}_1} > 820$ GeV,
- charged slepton masses $m_{\tilde{l}} > 240$ GeV,
- sneutrino masses $m_{\tilde{\nu}} > 400$ GeV,
- wino-like chargino masses $m_{\tilde{\chi}_1^\pm} > 450$ GeV.

It is obviously that above limits can be easily escaped through chosing heavy gluino and squarks and arranging the mixing matrix of charginos. Moreover, noticed that we assumed the relevant couplings λ_1 is negligible in our model. Therefore, these bounds are still relaxed significantly even we do not apply the heavy spectrum. Similarly, constraints based on LQD^c operators also do not threat our model since the relevant searches are mainly investigated with stop-pair production and setting stop masses up to 1 TeV. Based on above discussion, we choose $m_{\tilde{\chi}^\pm,\tilde{\chi}^0}=350$ (800) GeV for the case of light (heavy) electroweakinos, and taking gluino and squarks are heavier than 1 TeV. In order to extract the key features from the parameter space, we further make following assumption:

- The soft trilinear couplings T_{λ_1} are fixed as $T_{\lambda_1}^{122}=T_{\lambda_1}^{133}=10$ TeV.
- Due to the PDF dependence, the luminosity ratios between 8 TeV and 13 TeV are distinct for first and second generation quarks. It is then interesting to examine their contributions separately. For this aim, We treated λ_2^{111} and λ_2^{122} as independent operators. Furthermore, the non-diagonal couplings λ_2^{112} and and λ_2^{121} are combined as a single operator (labeled by $\lambda_2^{12,21}$) with $\lambda_2^{112}=\lambda_2^{121}$ to account for mixed contributions of first two generation quarks. In the numerical calculation, we assume that each operators contributes one at a time. Finally , we use $\lambda_2^{\rm tot}$ to denote the universal couplings with $\lambda_2^{111}=\lambda_2^{122}=\lambda_2^{112}=\lambda_2^{121}$.

In table I, we list cross sections of sneutrino production at LHC 13 TeV (8 TeV) respectively correspond to couplings λ_2^{111}, λ_2^{122}, $\lambda_2^{112,21}$ and $\lambda_2^{\rm tot}$. Where the typical value is taken as $|\lambda_2|=1$. Their cross sections fall into the region $\mathcal{O}(10-100)$ pb and possessing following order,

$$\sigma^{13\mathrm{TeV}}_{pp\to\tilde{\nu}_e}(\lambda_2^{111}) > \sigma^{13\mathrm{TeV}}_{pp\to\tilde{\nu}_e}(\lambda_2^{112,21}) > \sigma^{13\mathrm{TeV}}_{pp\to\tilde{\nu}_e}(\lambda_2^{122}). \tag{14}$$

Which is resulted from PDF dependence of first and second generation quarks. In the narrow width approximation, the diphoton signal rate can be calculated as

$$\sigma^{13\mathrm{TeV}}_{pp\to\gamma\gamma} \simeq \sigma^{13\mathrm{TeV}}_{pp\to\tilde{\nu}_e}|\lambda_2^{1jk}|^2\cdot \mathrm{BR}_{\gamma\gamma}. \tag{15}$$

Currently, the most stringent LHC constraint for our model coming from dijet and diphoton resonance searches performed at LHC 8 TeV. Corresponding upper bounds at 95% confidence level yield $\sigma^{8\text{TeV}}_{pp\to jj} < 2.5$ pb [48] and $\sigma^{8\text{TeV}}_{pp\to\gamma\gamma} < 1.5$ fb [49, 50], respectively. Since they have different impact on the model parameter space, we discuss them one by one. We start with dijet constraint. The cross section of dijet final states resulted from $\tilde{\nu}_e$ decay is given by,

$$\sigma^{8\text{TeV}}_{pp\to jj} \simeq \sigma^{8\text{TeV}}_{pp\to\tilde{\nu}_e}|\lambda_2^{1jk}|^2 \cdot \text{BR}_{d\bar{d}}, \tag{16}$$

In addition, selectron decay $\tilde{e}_L^{\pm} \to u_j\bar{d}_k/\bar{u}_j d_k$ also contributes to dijet final states. Whose cross section can be well approximated by,

$$\begin{aligned}\sigma(pp\to\tilde{e}_L^- \to \bar{u}_j d_k) &\simeq \sigma^{8\text{TeV}}_{pp\to\tilde{e}_L^-}|\lambda_2^{1jk}|^2 \cdot \text{BR}_{\bar{u}d},\\ \sigma(pp\to\tilde{e}_L^+ \to u_j\bar{d}_k) &\simeq \sigma^{8\text{TeV}}_{pp\to\tilde{e}_L^+}|\lambda_2^{1jk}|^2 \cdot \text{BR}_{u\bar{d}}.\end{aligned} \tag{17}$$

Where $\text{BR}_{\bar{u}d\ (u\bar{d})} = \Gamma_{\bar{u}d\ (u\bar{d})}/(\Gamma_{\bar{u}d\ (u\bar{d})} + \Gamma_{\chi l})$. $\Gamma_{\bar{u}d\ (u\bar{d})}$ and $\Gamma_{\chi l}$ are obtained by replacing $m_{\tilde{\nu}_e}$ in Eq. 12 and 13 to $m_{\tilde{e}_L^{\mp}}$, respectively. In Eq. 17, we have ignored the loop-induced decay modes WZ and $W\gamma$ since they are high suppressed compared with tree-level ones. Notice that the mass splitting for the left-handed slpeton are determined by model independent relation $m^2_{\tilde{e}_L} - m^2_{\tilde{\nu}_e} = -\cos(2\beta)m^2_W$ [51], we thus have $m_{\tilde{e}_L^{\pm}} = 754$ GeV for $m_{\tilde{\nu}_e} = 750$ GeV and $\tan\beta = 10$. Which indicates contribution coming from $\tilde{e}_L^{\pm}$ must be taken into account since their masses are close to $\tilde{\nu}_e$. Similar to table I, cross sections of $\tilde{e}_L^{\pm}$ production at LHC 8 TeV are listed in table II.

We first investigate the case of light electroweakinos. We require that signal cross sections respectively satisfy the CMS and ATLAS observations which are listed in Eq. 1, with imposing the dijet upper bound $\sigma^{8\text{TeV}}_{pp\to jj} < 2.5$ pb. In figure 1 and 2, we respectively display the allowed regions for each independent operator in $[m_{\tilde{\mu},\tilde{\tau}},\ \lambda_2^{ijk}]$ plane for CMS and ATLAS observations. In addition, the largest total decay width can be reached in each parameter regions are also shown. There are some important results can be learned from these figures:

- All the independent couplings can fit the CMS observation. The upper bounds of allowed regions for different couplings λ_2 have inverse hierarchy with that of production rate in Eq. 14 since a smaller production cross section makes a larger upper bound of coupling. Furthermore, λ_2^{111} and $\lambda_2^{112,21}$ give roughly comparable parameter space while λ_2^{122} and λ_2^{tot} coupling hold relatively small regions. Which is due to the fact that λ_2^{122} has the smallest production cross section, making it can only fit the signal rate in a narrow mass regions. On the other hand, λ_2^{tot} gives the largest senutrino production with the smallest diphoton branching ratio. As a result, it takes moderate diphoton signal rate. While the dijet constraint is most stringent for λ_2^{tot}, thus significantly reduces its parameter space.

- For ATLAS observation, only λ_2^{111} and $\lambda_2^{112,21}$ couplings are survived with tiny parameter space while λ_2^{122} and λ_2^{tot} couplings are totally excluded. This can be explained as follows: ATLAS observation prefer large signal cross section, while senutrino production resulted from λ_2^{122} coupling is too small to reach such signal rate. On the other hand, for λ_2^{tot} coupling, the reason is similar with the case of CMS. But for ATLAS case, required diphoton signal rate and dijet limit can never be balanced thus totally exclude λ_2^{tot} in whole parameter space.

- The largest total decay width corresponding to CMS (ATLAS) observation is about 30 (14) GeV, which is provided by λ_2^{122} ($\lambda_2^{112,21}$) coupling. Especially, best-fit width $\Gamma_{\text{tot}} = 45$ GeV suggested by ATLAS observation can never be satisfied in our parameter space.

Production cross section (pb)	λ_2^{111}	λ_2^{122}	$\lambda_2^{112,21}$	λ_2^{tot}
$\sigma^{13\text{TeV}}_{pp\to\tilde{\nu}_e}$	77.6	9.6	68.3	155.4
$\sigma^{8\text{TeV}}_{pp\to\tilde{\nu}_e}$	30	2.3	22.2	54.6

TABLE I. Production cross sections of $\tilde{\nu}_e$ at LHC 13 TeV and 8 TeV respectively correspond to couplings λ_2^{111}, λ_2^{122}, $\lambda_2^{112,21}$ and λ_2^{tot}. Where the typical value is taken to be $|\lambda_2| = 1$.

Production cross section (pb)	λ_2^{111}	λ_2^{122}	$\lambda_2^{112,21}$	λ_2^{tot}
$\sigma^{8\text{TeV}}_{pp\to\tilde{e}_L^-}$	23.1	1.4	15.2	45.9
$\sigma^{8\text{TeV}}_{pp\to\tilde{e}_L^+}$	58.1	3.2	41.5	144.6

TABLE II. Similar with table I, but for $\tilde{e}_L^{\pm}$ at LHC 8 TeV.

We further address constraint from diphoton channel. Since current upper limit for this channel is $\sigma^{8\text{TeV}}_{pp\to\gamma\gamma} < 1.5$ fb, compatibility of diphoton excess between LHC 8 TeV and 13 TeV has to be examed. In figure 3, we present allowed parameter space in the same plane with imposing both dijet and diphoton constraints. where the diphoton signal rate at LHC 8 TeV is computed as

$$\sigma^{8\text{TeV}}_{pp\to\gamma\gamma} \simeq \sigma^{8\text{TeV}}_{pp\to\tilde{\nu}_e}|\lambda_2^{1jk}|^2 \cdot \text{BR}_{\gamma\gamma}. \tag{18}$$

In this case, we find that the parameter space for ATLAS observation is entirely ruled out. Even for CMS result, allowed parameter regions for different couplings are also changed dramatically. To be specific, the parameter space is disappeared for λ_2^{tot} coupling; getting smaller for λ_2^{111} and $\lambda_2^{112,21}$ couplings; while keeping almost unchanged for λ_2^{122} coupling. To understand such behaviors, one noticed that the growth of production cross sections at LHC 13 TeV and 8 TeV are different for the

first and second generation quarks. From table I, we find that the increasing of cross sections for $\tilde{\nu}_e$ production are given by,

$$\frac{\sigma^{13}_{pp\to\tilde{\nu}_e}}{\sigma^{8}_{pp\to\tilde{\nu}_e}}(\lambda_2^{111}) \simeq 2.58,\ \frac{\sigma^{13}_{pp\to\tilde{\nu}_e}}{\sigma^{8}_{pp\to\tilde{\nu}_e}}(\lambda_2^{112,21}) \simeq 3.07,$$
$$\frac{\sigma^{13}_{pp\to\tilde{\nu}_e}}{\sigma^{8}_{pp\to\tilde{\nu}_e}}(\lambda_2^{122}) \simeq 4.17,\ \frac{\sigma^{13}_{pp\to\tilde{\nu}_e}}{\sigma^{8}_{pp\to\tilde{\nu}_e}}(\lambda_2^{\rm tot}) \simeq 2.85. \qquad (19)$$

Due to different PDF dependence, the growth ratio for second generation quarks are higher than that of first generation, leading to the couplings involved with second generation quarks (λ_2^{122} and $\lambda_2^{112,21}$) have more significant increasing on signal rate. Meanwhile, the growth of observed diphoton signal rate from LHC 8 TeV to 13 TeV are estimated as

$$\frac{\sigma^{13\rm TeV}_{pp\to\gamma\gamma}}{\sigma^{8\rm TeV}_{pp\to\gamma\gamma}} \simeq \begin{cases} \frac{(10\pm3)\ \rm fb}{1.5\ \rm fb} \sim 4.7-8.7 & \text{for ATLAS,} \\ \frac{(6\pm3)\ \rm fb}{1.5\ \rm fb} \sim 2-6 & \text{for CMS.} \end{cases} \qquad (20)$$

Based on Eq. 19 and 20, it is clearly that none of couplings in our model can fit the ATLAS observation and simultaneously guarantee the compatibility of diphoton excess between LHC 8 TeV and 13 TeV. On the other hand, the situation is much better for CMS observation. In this case, couplings λ_2^{122} and $\lambda_2^{112,21}$ are more advantageous since they are benefit from large growth ratio of second generation quarks, thus preserving the compatibility of diphoton excess as much as possible. While for λ_2^{111} coupling which only involved with first generation quarks, whose increasing of cross section is slightly larger than the lower bound of growth of CMS diphoton signal rate, thus disfavored by compatibility of diphoton excess. Finally, coupling $\lambda_2^{\rm tot}$ is totally excluded due to stringent dijet bound although possessing second smallest of increasing.

Next, we briefly discuss the case of heavy electroweakinos. The remarkable difference is that the decay mode related to electroweakinos is kinematically forbidden in this case, leading to $\Gamma_{\chi l} = 0$. Which clearly enhances the branching ratio of diphoton mode, while with the price of reducing total decay width. Similar with the case of light electroweakinos, the parameter space for ATLAS observation is also disappeared after imposing both dijet and diphoton constraints at LHC 8 TeV. We thus only present results on CMS observation in Fig. 4. The changing of parameter space are summarized as follows:

- the allowed mass regions for smuon/stau are extended up to about 480 GeV,
- the largest total decay width in each parameter regions are correspondingly reduced. For instance, $\Gamma_{\rm tot}$ respectively drop to 17 GeV and 1 GeV for λ_2^{122} and λ_2^{111}.

Before ending up this section, we mention that the parameter space of λ_2 in Figs. 3 and 4 should be also consistent with the exisiting low-energy constraints. The indirect bounds coming from various low energy experiments are collected in Ref. [38], those most related to our model are listed blow [1]:

$$\begin{aligned}
\lambda_2^{111} &\le 5\times10^{-4}\left(\frac{m_{\tilde{f}}}{100\ \rm GeV}\right)^2\left(\frac{m_{\tilde{g}/\tilde{\chi}}}{100\ \rm GeV}\right)^{\frac{1}{2}}\ [\beta\beta0\nu], \\
\lambda_2^{11k} &\le 0.02\left(\frac{m_{\tilde{d}_{kR}}}{100\ \rm GeV}\right)\ [V_{ud}], \\
\lambda_2^{12k} &\le 0.21\left(\frac{m_{\tilde{d}_{kR}}}{100\ \rm GeV}\right)\ [A_{FB}], \\
\lambda_2^{1j1} &\le 0.03\left(\frac{m_{\tilde{u}_{jL}}}{100\ \rm GeV}\right)\ [Q_W(\rm Cs)]. \qquad (21)
\end{aligned}$$

In above equation, $m_{\tilde{f}}$ and $m_{\tilde{g}/\tilde{\chi}}$ respectively denote sfermion, gluino/neutralino masses. The notations in the brackets stand for the corresponding low-energy constraints which are illustrated as follows:

- $\beta\beta0\nu$: neutrinoless double beta decay of nuclei, constraining by the lower limit on the half-life of ^{76}Ge isotope [52] [53];
- V_{ud}: charged current universality in the quark sector, constraining by the experimental value of the CKM matrix element V_{ud} [54];
- A_{FB}: forward-backward asymmetries of fermion pair production process via Z boson resonant $e^+e^-\to Z^0\to f\bar{f}$, constraining through the experimental values of A^f_{FB} measured by CERN LEP-I [54];
- Q_W(Cs): deviation of the weak charge Q_W to its SM value, constraining by the parity violating transitions in ^{133}Cs [55] [56].

One can see that most of low-energy constraints rely on squark and gluino masses which are decoupled in our spectrum, thus are harmless for the parameter space of λ_2. The only threatening constraint coming from the $\beta\beta0\nu$, which involved with charged slepton and neutralino masses thus imposing very stringent bound on λ_2^{111}. In the case of light electroweakinos with $(m_{\tilde{e}_L},\ m_{\tilde{\chi}^0}) = (754,\ 350)$ GeV, the first equation of Eq. 21 implies $\lambda_2^{111} \le 0.053$. As a consequence, the allowed regions for λ_2^{111} in Figs. 3 are totally excluded. On the other hand, for light electroweakinos with $(m_{\tilde{e}_L},\ m_{\tilde{\chi}^0}) = (754,\ 800)$ GeV, the corresponding limit is $\lambda_2^{111} \le 0.08$. Which still allowing some parameter space for λ_2^{111} and $\lambda_2^{\rm tot}$.

Conclusion–In summary, we have proposed an supersymmetric explanation of the diphoton excess within the

[1] We do not include limit coming from the neutrino masses and mixings since which relys on assumptions of the generation structure of λ_2 [38], which are not specified in our model. In addition, we adopt more recent result in Ref. [53] for limit from neutrinoless double beta decay.

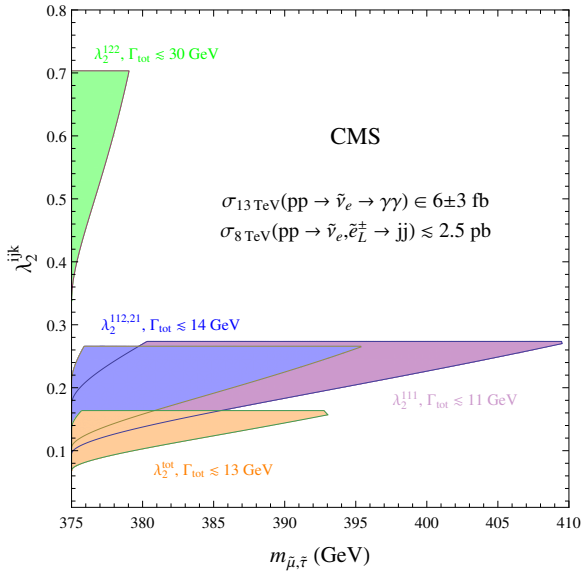
λ_2^{122}, $\Gamma_{\rm tot} \lesssim 30$ GeV
CMS
$\sigma_{13\,\rm TeV}(pp \to \tilde{\nu}_e \to \gamma\gamma) \in 6\pm3$ fb
$\sigma_{8\,\rm TeV}(pp \to \tilde{\nu}_e, \tilde{e}_L^{\pm} \to jj) \lesssim 2.5$ pb
$\lambda_2^{112,21}$, $\Gamma_{\rm tot} \lesssim 14$ GeV
λ_2^{111}, $\Gamma_{\rm tot} \lesssim 11$ GeV
$\lambda_2^{\rm tot}$, $\Gamma_{\rm tot} \lesssim 13$ GeV
λ_2^{ijk}
$m_{\tilde{\mu},\tilde{\tau}}$ (GeV)

FIG. 1. The allowed region for the diphoton excess required by CMS observation on the $[m_{\tilde{\mu},\tilde{\tau}},\ \lambda_2^{ijk}]$ plane with only considering constraint from dijet constraint at 8 TeV LHC. Here the mass of electroweakinos are fixed as $m_{\tilde{\chi}^{\pm},\tilde{\chi}^0} = 350$ GeV. The regions with purple, green, blue and orange color correspond to contributions of λ_2^{111}, λ_2^{122}, $\lambda_2^{112,21}$ and $\lambda_2^{\rm tot}$, respectively. For comparison, the largest total decay width for each parameter region is also shown.

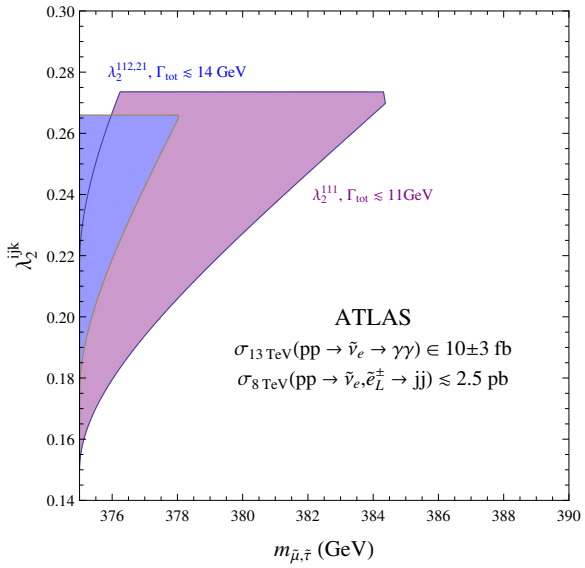
$\lambda_2^{112,21}$, $\Gamma_{\rm tot} \lesssim 14$ GeV
λ_2^{111}, $\Gamma_{\rm tot} \lesssim 11$GeV
ATLAS
$\sigma_{13\,\rm TeV}(pp \to \tilde{\nu}_e \to \gamma\gamma) \in 10\pm3$ fb
$\sigma_{8\,\rm TeV}(pp \to \tilde{\nu}_e, \tilde{e}_L^{\pm} \to jj) \lesssim 2.5$ pb
λ_2^{ijk}
$m_{\tilde{\mu},\tilde{\tau}}$ (GeV)

FIG. 2. Similar with figure 1, but for the ATLAS observation. Notice that in this case the parameter space for λ_2^{122} and $\lambda_2^{\rm tot}$ are totally excluded thus do not presented here.

framework of LRPV MSSM. Where the 750 GeV resonance is identified as sneutrino and produced by $q\bar{q}$ initial state. With introducing relatively large trilinear soft parameter $T_{\lambda_1}^{1jj}$, the branching ratio of diphoton mode

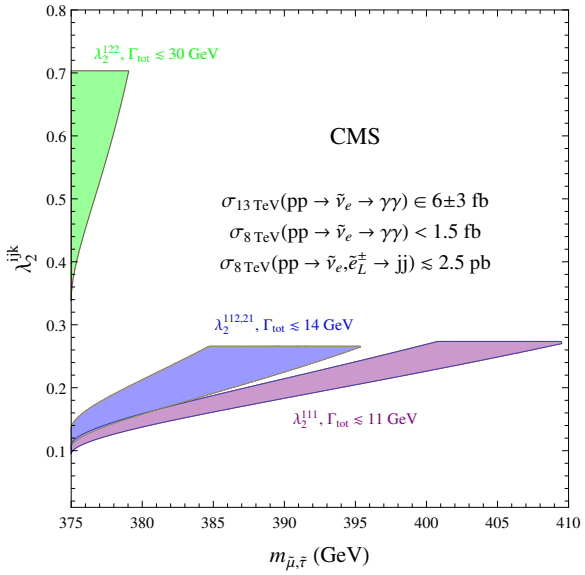
λ_2^{122}, $\Gamma_{\rm tot} \lesssim 30$ GeV
CMS
$\sigma_{13\,\rm TeV}(pp \to \tilde{\nu}_e \to \gamma\gamma) \in 6\pm3$ fb
$\sigma_{8\,\rm TeV}(pp \to \tilde{\nu}_e \to \gamma\gamma) < 1.5$ fb
$\sigma_{8\,\rm TeV}(pp \to \tilde{\nu}_e, \tilde{e}_L^{\pm} \to jj) \lesssim 2.5$ pb
$\lambda_2^{112,21}$, $\Gamma_{\rm tot} \lesssim 14$ GeV
λ_2^{111}, $\Gamma_{\rm tot} \lesssim 11$ GeV
λ_2^{ijk}
$m_{\tilde{\mu},\tilde{\tau}}$ (GeV)

FIG. 3. The allowed region for the diphoton excess required by CMS observation on the $[m_{\tilde{\mu},\tilde{\tau}},\ \lambda_2^{ijk}]$ plane with considering both dijet and diphoton constraints at 8 TeV LHC.

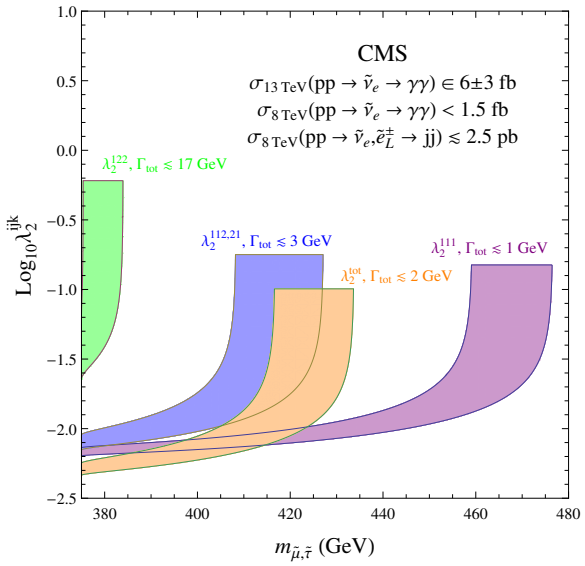
CMS
$\sigma_{13\,\rm TeV}(pp \to \tilde{\nu}_e \to \gamma\gamma) \in 6\pm3$ fb
$\sigma_{8\,\rm TeV}(pp \to \tilde{\nu}_e \to \gamma\gamma) < 1.5$ fb
$\sigma_{8\,\rm TeV}(pp \to \tilde{\nu}_e, \tilde{e}_L^{\pm} \to jj) \lesssim 2.5$ pb
λ_2^{122}, $\Gamma_{\rm tot} \lesssim 17$ GeV
$\lambda_2^{112,21}$, $\Gamma_{\rm tot} \lesssim 3$ GeV
λ_2^{111}, $\Gamma_{\rm tot} \lesssim 1$ GeV
$\lambda_2^{\rm tot}$, $\Gamma_{\rm tot} \lesssim 2$ GeV
$\rm Log_{10}\lambda_2^{ijk}$
$m_{\tilde{\mu},\tilde{\tau}}$ (GeV)

FIG. 4. The allowed region for the diphoton excess required by CMS observation on the $[m_{\tilde{\mu},\tilde{\tau}},\ \log\lambda_2^{ijk}]$ plane with considering constraints from both dijet and diphoton resonance searches. Here the mass of electroweakinos are fixed as $m_{\tilde{\chi}^{\pm},\tilde{\chi}^0} = 800$ GeV.

received significantly enhancement compared with conventional MSSM. The important features and predictions of our model are summarized as follows:

- In our model, the sneutrino resonance is produced via $q\bar{q}$ annihilation. Which is distinct from models produced by gg initial state. The two production

channel can be distinguished in principle by using angular distributions with sufficiently large statistics.

- With considering dijet and diphoton constraints at LHC 8 TeV, our model can successfully fit the CMS data in sizeable parameter regions. While for large signal cross section and a width of 45 GeV suggested by ATLAS data, the parameter space is entirely ruled out. Fitting the excess strongly favors the mass of stau and smuon within the range of $375 - 410$ $(375 - 480)$ GeV for the case of light (heavy) electroweakinos. Which is a strong prediction for mass spectrum of slepton sector.

- The predicted total decay width can reaches 30 (17) GeV for light (heavy) electroweakinos.

- The low-energy constraint from neutrinoless double beta decay imposes severe bound on coupling λ_2^{111}. Combined with the compatibility of diphoton excess between LHC 8 TeV and 13 TeV, the couplings involved with second generation quarks have more advantages.

Note added– After a few days we submitted our paper to arXiv, Ref. [57] appeared, which explains the diphoton excess using the similar scenario. The difference is that the authors consider degenerate electron or moun sneutrino as the resonance and producing only through first generation quarks. In addition, they do not discuss the compatibility of diphoton excess between LHC 8 TeV and 13 TeV.

Acknowledgements– This research was supported in part by the Natural Science Foundation of China under grant numbers 11135003, 11275246, and 11475238 (TL).

[1] The ATLAS collaboration, ATLAS-CONF-2015-081.
[2] CMS note, CMS PAS EXO-15-004, "Search for new physics in high mass diphoton events in proton-proton collisions at 13 TeV".
[3] R. Franceschini *et al.*, arXiv:1512.04933 [hep-ph].
[4] A. Pilaftsis, arXiv:1512.04931 [hep-ph].
[5] D. Buttazzo, A. Greljo and D. Marzocca, arXiv:1512.04929 [hep-ph].
[6] S. Knapen, T. Melia, M. Papucci and K. Zurek, arXiv:1512.04928 [hep-ph].
[7] A. Angelescu, A. Djouadi and G. Moreau, arXiv:1512.04921 [hep-ph].
[8] Y. Nakai, R. Sato and K. Tobioka, arXiv:1512.04924 [hep-ph].
[9] M. Backovic, A. Mariotti and D. Redigolo, arXiv:1512.04917 [hep-ph].
[10] Y. Mambrini, G. Arcadi and A. Djouadi, arXiv:1512.04913 [hep-ph].
[11] K. Harigaya and Y. Nomura, arXiv:1512.04850 [hep-ph].
[12] E. Molinaro, F. Sannino and N. Vignaroli, arXiv:1512.05334 [hep-ph].
[13] C. Petersson and R. Torre, arXiv:1512.05333 [hep-ph].
[14] R. S. Gupta, S. Jäger, Y. Kats, G. Perez and E. Stamou, arXiv:1512.05332 [hep-ph].
[15] B. Bellazzini, R. Franceschini, F. Sala and J. Serra, arXiv:1512.05330 [hep-ph].
[16] M. Low, A. Tesi and L. T. Wang, arXiv:1512.05328 [hep-ph].
[17] J. Ellis, S. A. R. Ellis, J. Quevillon, V. Sanz and T. You, arXiv:1512.05327 [hep-ph].
[18] S. D. McDermott, P. Meade and H. Ramani, arXiv:1512.05326 [hep-ph].
[19] T. Higaki, K. S. Jeong, N. Kitajima and F. Takahashi, arXiv:1512.05295 [hep-ph].
[20] Y. Bai, J. Berger and R. Lu, arXiv:1512.05779 [hep-ph].
[21] D. Aloni, K. Blum, A. Dery, A. Efrati and Y. Nir, arXiv:1512.05778 [hep-ph].
[22] A. Falkowski, O. Slone and T. Volansky, arXiv:1512.05777 [hep-ph].
[23] C. Csaki, J. Hubisz and J. Terning, arXiv:1512.05776 [hep-ph].
[24] P. Agrawal, J. Fan, B. Heidenreich, M. Reece and M. Strassler, arXiv:1512.05775 [hep-ph].
[25] A. Ahmed, B. M. Dillon, B. Grzadkowski, J. F. Gunion and Y. Jiang, arXiv:1512.05771 [hep-ph].
[26] J. Chakrabortty, A. Choudhury, P. Ghosh, S. Mondal and T. Srivastava, arXiv:1512.05767 [hep-ph].
[27] L. Bian, N. Chen, D. Liu and J. Shu, arXiv:1512.05759 [hep-ph].
[28] D. Curtin and C. B. Verhaaren, arXiv:1512.05753 [hep-ph].
[29] S. Fichet, G. von Gersdorff and C. Royon, arXiv:1512.05751 [hep-ph].
[30] W. Chao, R. Huo and J. H. Yu, arXiv:1512.05738 [hep-ph].
[31] S. V. Demidov and D. S. Gorbunov, arXiv:1512.05723 [hep-ph].
[32] J. M. No, V. Sanz and J. Setford, arXiv:1512.05700 [hep-ph].
[33] D. Becirevic, E. Bertuzzo, O. Sumensari and R. Z. Funchal, arXiv:1512.05623 [hep-ph].
[34] P. Cox, A. D. Medina, T. S. Ray and A. Spray, arXiv:1512.05618 [hep-ph].
[35] A. Kobakhidze, F. Wang, L. Wu, J. M. Yang and M. Zhang, arXiv:1512.05585 [hep-ph].
[36] S. Matsuzaki and K. Yamawaki, arXiv:1512.05564 [hep-ph].
[37] B. Dutta, Y. Gao, T. Ghosh, I. Gogoladze and T. Li, arXiv:1512.05439 [hep-ph].
[38] R. Barbier *et al.*, Phys. Rept. **420**, 1 (2005) doi:10.1016/j.physrep.2005.08.006 [hep-ph/0406039].
[39] S. Bar-Shalom, G. Eilam, J. Wudka and A. Soni, Phys. Rev. D **59**, 035010 (1999) doi:10.1103/PhysRevD.59.035010 [hep-ph/9809253].
[40] J. F. Gunion, H. E. Haber, G. L. Kane and S. Dawson, Front. Phys. **80**, 1 (2000).
[41] V. D. Barger, G. F. Giudice and T. Han, Phys. Rev. D **40**, 2987 (1989). doi:10.1103/PhysRevD.40.2987
[42] F. Staub, Comput. Phys. Commun. **184**, 1792 (2013) doi:10.1016/j.cpc.2013.02.019 [arXiv:1207.0906

[hep-ph]]. F. Staub, Comput. Phys. Commun. **185**, 1773 (2014) doi:10.1016/j.cpc.2014.02.018 [arXiv:1309.7223 [hep-ph]].
[43]
[43] C. Degrande, C. Duhr, B. Fuks, D. Grellscheid, O. Mattelaer and T. Reiter, Comput. Phys. Commun. **183**, 1201 (2012) [arXiv:1108.2040 [hep-ph]].
[44] J. Alwall, M. Herquet, F. Maltoni, O. Mattelaer and T. Stelzer, JHEP **1106**, 128 (2011) [arXiv:1106.0522 [hep-ph]]; J. Alwall, R. Frederix, S. Frixione, V. Hirschi, F. Maltoni, O. Mattelaer, H.-S. Shao and T. Stelzer *et al.*, JHEP **1407**, 079 (2014) [arXiv:1405.0301 [hep-ph]].
[45] P. M. Nadolsky, H. L. Lai, Q. H. Cao, J. Huston, J. Pumplin, D. Stump, W. K. Tung and C.-P. Yuan, Phys. Rev. D **78**, 013004 (2008) doi:10.1103/PhysRevD.78.013004 [arXiv:0802.0007 [hep-ph]].
[46] A. Redelbach, Advances in High Energy Physics, vol. 2015, Article ID 982167, 2015 [arXiv:1512.05956 [hep-ex]].
[47] G. Aad *et al.* [ATLAS Collaboration], Phys. Rev. D **90**, no. 5, 052005 (2014) doi:10.1103/PhysRevD.90.052005 [arXiv:1405.4123 [hep-ex]].
[48] CMS Collaboration [CMS Collaboration], CMS-PAS-EXO-14-005.
[49] G. Aad *et al.* [ATLAS Collaboration], Phys. Rev. D **92**, no. 3, 032004 (2015) doi:10.1103/PhysRevD.92.032004 [arXiv:1504.05511 [hep-ex]].
[50] CMS Collaboration [CMS Collaboration], CMS-PAS-HIG-14-006.
[51] S. P. Martin, Adv. Ser. Direct. High Energy Phys. **21**, 1 (2010) [Adv. Ser. Direct. High Energy Phys. **18**, 1 (1998)] [hep-ph/9709356].
[52] H. V. Klapdor-Kleingrothaus *et al.*, Eur. Phys. J. A **12**, 147 (2001) doi:10.1007/s100500170022 [hep-ph/0103062].
[53] B. C. Allanach, C. H. Kom and H. Pas, JHEP **0910**, 026 (2009) doi:10.1088/1126-6708/2009/10/026 [arXiv:0903.0347 [hep-ph]].
[54] K. Hagiwara *et al.* [Particle Data Group Collaboration], Phys. Rev. D **66**, 010001 (2002). doi:10.1103/PhysRevD.66.010001
[55] J. L. Rosner, Phys. Rev. D **65**, 073026 (2002) doi:10.1103/PhysRevD.65.073026 [hep-ph/0109239].
[56] J. S. M. Ginges and V. V. Flambaum, Phys. Rept. **397**, 63 (2004) doi:10.1016/j.physrep.2004.03.005 [physics/0309054].
[57] B. C. Allanach, P. S. B. Dev, S. A. Renner and K. Sakurai, arXiv:1512.07645 [hep-ph].